

# **A simple algorithm for sequentially incorporating gravity observations in seismic traveltimes tomography**

Tom Parsons

U. S. Geological Survey, MS-999, 345 Middlefield Rd. Menlo Park, California 94025  
tparsons@usgs.gov

Richard J. Blakely

U. S. Geological Survey, MS-989, 345 Middlefield Rd. Menlo Park, California 94025  
blakely@usgs.gov

Thomas M. Brocher

U. S. Geological Survey, MS-977, 345 Middlefield Rd. Menlo Park, California 94025  
brocher@usgs.gov

## **Abstract.**

The geologic structure of the Earth's upper crust can be revealed by modeling variation in seismic arrival times and in potential field measurements. We demonstrate a simple method for sequentially satisfying seismic traveltimes and observed gravity residuals in an iterative 3-D inversion. The algorithm is portable to any seismic analysis method that uses a gridded representation of velocity structure. Our technique calculates the gravity anomaly resulting from a velocity model by converting to density with Gardner's rule. The residual between calculated and observed gravity is minimized by weighted adjustments to the model velocity-depth gradient where the gradient is steepest and where seismic coverage is least. The adjustments are scaled by the sign and magnitude of the gravity residuals, and a smoothing step is performed to minimize vertical streaking. The adjusted model is then used as a starting model in the next seismic traveltimes iteration. The process is repeated until one velocity model can simultaneously satisfy both the gravity anomaly and seismic traveltimes observations within acceptable misfits. We test our algorithm with data gathered in the Puget Lowland of Washington State, USA (Seismic Hazards Investigation in Puget Sound (SHIPS) experiment). We perform resolution tests with synthetic traveltimes and gravity observations calculated with a checkerboard velocity model using the SHIPS experiment geometry and show that the addition of gravity significantly enhances resolution. We calculate a new velocity model for the region using SHIPS traveltimes and observed gravity, and show examples where correlation between surface geology and modeled subsurface velocity structure is enhanced.

## Introduction

Three-dimensional tomographic studies of the Earth's crust using local seismic arrival times has become increasingly common (e.g., Iyer and Hirahara, 1993). Less common has been systematic use of gravity observations to constrain 3-D crustal seismic models, or generation of a single model that is consistent with seismic traveltimes and the gravity anomaly. Tomography and gravity methods complement each other in various ways. Gravity anomalies decrease in amplitude and increase in wavelength with increasing source depth. Thus, gravity inversions have greatest resolving power at shallow depths, where wide-angle seismic methods are typically less effective. Moreover, gravity anomalies are sensitive to lateral variations in mass distribution, but resolving changes with depth with gravity data can prove challenging. Seismic methods, on the other hand, are effective in resolving vertical variations. Often, gravity measurements outnumber seismic recorders in a given area, and are differently distributed. By combining gravity and tomography, we anticipate that we will capitalize on the strengths of each method. We thus seek a method to incorporate gravity analysis into seismic tomography that is easy to implement and that is readily adaptable to different seismic modeling techniques.

Simultaneous, or quasi-simultaneous inversion of seismic traveltime and observed gravity residuals in an inversion is not a new concept. Past work can be classified in three ways (Golizdra, 1980): (1) tests of final seismic velocity models for consistency with gravity; (2) joint inversions for gravity and traveltimes; and (3) sequential inversions (alternating gravity and traveltime steps; Lines (1988)). Gravity constraints are most often employed by conversion of a simplified seismic velocity model to density, and calculation of the gravity anomaly for comparison with observed measurements (e.g., Achauer, 1992; Luetgert, 1992; Masson et al., 1998; Brocher et al., 2001; Langenheim and Hauksson, 2001). Such modeling tests seismic models and can highlight regions of the crust that have anomalous velocity-density relations. However, since seismic models are often simplified for use with layer- or polygon-based gravity modeling methods, potential improvements in resolution from incorporating gravity analysis may not be fully exploited.

Joint seismic-gravity inversion techniques (e.g., Oppenheimer and Herkenhoff, 1981; Hammer, 1991; Lees and VanDecar, 1991) have the benefit of true simultaneous consideration of the traveltime and gravity residuals that minimizes bias from either constraint. However, they

require a linear approximation to the relation between gravity and seismic velocity (Lines, 1988; Lees and VanDecar, 1991) and involve a loss of flexibility because a single algorithm must be used. Options available to the modeler of seismic traveltimes are burgeoning, with many taking advantage of fast finite-difference traveltime calculation schemes (e.g., Vidale, 1990).

In this paper we present a technique for sequential inversion of seismic traveltime and gravity residuals. Our motivation is to sharpen velocity images of the upper and middle crust from controlled and local earthquake tomography by exploiting superior spatial density of gravity observations. We provide a flexible algorithm that can be applied with any grid-based seismic analysis method. Our sequential inversion is semi-coupled like that of Lines (1988), except that instead of fixed velocity-density boundaries with an uncoupled velocity-density relation, we fix the velocity-density relation and move velocity-depth gradients.

## Method

In this study, observed gravity is incorporated as a sequential step in the inversion process. Thus our method is not a joint inversion in a rigorous sense, where residuals from traveltime and gravity are minimized simultaneously through a linear expression that relates the two. Instead, the gravitational field predicted by a velocity model obtained from traveltime inversion is compared with observed gravity. Velocities are modified to reduce residuals, and used as the starting model for the next traveltime iteration. A fixed velocity-density relation enables all output models to be expressed as both velocity and density; the technique could be readily modified to incorporate spatially variable velocity-density relations if desired.

For traveltime inversion we use the 3-D tomographic technique of Hole (1992) modified to simultaneously invert for velocity, hypocenters, and origin times (hypocenters and origin times only for the earthquake data). This technique applies a finite-difference solution to the eikonal equation (Vidale, 1990; updated by Hole and Zelt, 1995) to calculate first arrival times through a gridded slowness model. An iterative nonlinear inversion is performed as a backprojection along raypaths determined from the forward modeling step. The updated velocity model from traveltime inversions is passed to the gravity step as a starting model. In this study we apply the gravity algorithm sequentially in 3-D, but it can easily be adapted for use with any gridded, or node-based traveltime modeling method in 2-D or 3-D.

For the example presented here, the gravity anomaly is calculated on the first iteration of the velocity model by converting velocity to density using Gardner's non-linear rule of  $\rho = 1740v^{1/4}$  for velocities (in km/s) below 6 km/s (Gardner et al., 1974), and  $\rho = 2920 \text{ kg/m}^3$  for velocities greater than 6 km/s which correspond to the Crescent formation (Brocher et al., 2001) (Figure 1). These choices may be modified for other regions as necessary. The gravity anomaly  $g(x,y)$  of a three-dimensional density distribution  $\rho(x,y,z)$  is the sum of the effects of each individual layer of the model. Let  $\rho(x,y,z)$  be discretized by layers, so that  $\rho(x,y,z) = \rho_k(x,y)$ , direct the  $z$  axis downward, and denote the two-dimensional Fourier transform by

$$\mathcal{F}[f] = \iint_{\square} f(x',y') \exp(i(k_x x' + k_y y')) dx' dy' \quad (1)$$

where  $k_x$  and  $k_y$  are wavenumbers for the  $x$  and  $y$  directions, respectively. The gravity anomaly due to the entire density distribution is given by

$$g(x,y) = \sum_{k=1}^N f_k(x,y) \quad (2)$$

where

$$\mathcal{F}[f_k] = \mathcal{F}[\rho_k] \cdot \mathcal{F}[e]. \quad (3)$$

The function  $\mathcal{F}[e]$  is the gravitational earth filter (Blakely, 1995) given by

$$\mathcal{F}[e] = \frac{2G}{k} (\exp(-kz_1) - \exp(-kz_2)), \quad z_1 > 0, \quad z_2 > z_1 \quad (4)$$

where  $G$  is the gravitational constant,  $z_1$  and  $z_2$  are depths to the top and bottom of layer  $k$ , respectively, and  $k = \sqrt{k_x^2 + k_y^2}$ . Thus, the gravity anomaly due to each layer was calculated by

(1) Fourier transforming the two-dimensional density of each layer, (2) multiplying by the appropriate earth filter, and (3) inverse Fourier transforming the product. Layers with uniform

density (inferred from uniform velocity) were ignored, as they would add only a constant to the overall anomaly.

The calculated anomaly is subtracted from observed gravity, which is gridded at the same scale as the top surface of the 3-D velocity model (1x1 km squares in this study), yielding a set of residual gravity values. The velocity model, represented by 1-km cubed cells of constant velocity and density, is then changed to minimize the residuals. A challenge is posed in fitting gravity observations because the observed anomaly at the surface is relatively independent of the depth of the source, yielding many possible models that satisfy the observations. We make some assumptions (as described below), and use constraints from seismic traveltime modeling to make targeted changes in the velocity-depth relation in each column in the velocity model. These changes result in a model that is consistent with observed gravity and seismic traveltimes.

Initially a grid of residual scaling factors is generated, each a function of the magnitude and sign of the corresponding residual gravity value, namely

$$R(x,y) = \frac{(r(x,y) \square \bar{r})}{\square} \quad (5)$$

where  $r(x,y)$  is the residual at a grid point,  $\bar{r}$  is the mean of all gravity residuals, and  $\square$  is an input constant used to scale the magnitude of velocity change. Larger values of  $\square$  cause smaller incremental changes in the velocity model with each iteration, allowing the effects of traveltime and gravity steps to gradually evolve a model consistent with both data sets. We arrived at appropriate  $\square$  values by experimenting with different numbers, using lowered RMS misfit in traveltime and gravity as the criterion.

The second step of the algorithm is calculation of the velocity-depth gradient ( $dV/dz$ ) at each model cell. The gradients are found by finite differencing the gridded velocity model. Gradient values are used to scale the velocity perturbations by maximizing changes where the gradients are highest, based on the assumption that much of the variation in the gravity anomaly results from sedimentary basin structures near the surface. Slight increases or decreases in the model depth to basement can quickly satisfy the residuals. In many cases, crustal tomography studies are undertaken to resolve basin structures (models for assessing likely earthquake strong ground motion for example). Preferentially changing velocity where gradients are highest has an effect

akin to subtly moving the depth to the basement-sediment interface. Subsequent traveltimes iterations allow such changes only within the allowable range that still satisfy the traveltimes data.

The last scale we apply on velocity perturbation resulting from gravity residuals is a seismic coverage factor. We scale the perturbations relative to the degree of calculated seismic ray coverage in a given model cell by

$$C(x,y,z) = 1 - \frac{h(x,y,z)}{H} \cdot \alpha \quad (6)$$

where  $h(x,y,z)$  is a hit count (number of times a seismic ray is calculated to encounter a model cell),  $H$  is the maximum hit count in the model, and  $\alpha$  is a weighting factor (can range from 0 to 1; we use a value of 0.1 in this study). Use of this scaling factor enables the model to be preserved where seismic coverage is high, and allows more variation where seismic coverage is low or nonexistent. Thus the gravity field can be used to supplement traveltimes coverage. The weighting value  $\alpha$  is an input parameter and allows control on how much weight to give the traveltimes data versus the gravity data. In our test cases we give most weight to seismic traveltimes because they are more sensitive to depth than residual gravity values, which are affected primarily by variations in basin structure.

Model velocity is changed by a simple product of the three scaling factors as

$$V^i(x,y,z) = V^o(x,y,z) + \frac{R(x,y)}{R} \cdot \left| \frac{dV^o(x,y,z)}{dz} \right| \cdot C(x,y,z) \cdot \frac{1}{C} \quad (7)$$

If any of the scaling factors approach zero at a given cell, then velocity is unchanged. Thus when the residuals grow very small, or when the velocity gradient is zero, the velocity perturbation approaches zero. The coverage scale  $C(x,y,z)$  is equal to 1 when the seismic hit count in a cell is zero (see equation 6), meaning that the perturbed velocity model is a function solely of the starting model and the gravity residuals in that case. Maximum and minimum allowable velocity-depth ranges are set that prevent unrealistic model velocities from developing. In this study, we set these ranges to the minima and maxima obtained from laboratory analysis at confining pressure of regional rock samples (Brocher et al., 2001). Lastly, a spatial smoothing filter is applied that minimizes vertical streaking, since perturbations are made column by column.

An example of the iterative process is shown in Figure 2. The largest changes in the velocity-depth curve occur at depths with steepest gradients and relatively little seismic coverage. The velocity-depth curve is slightly smoothed as a result of introducing the gravity constraint, especially where seismic coverage is minimal (Figure 2). This example is a representative column of the test model and traveltimes database (more fully discussed in a later section), and demonstrates the fairly minimal velocity perturbations necessary to satisfy both the traveltimes and the gravity anomalies.

### **Traveltimes database used to test method: The 1998 SHIPS experiment**

A traveltimes database from the Puget Lowland of Washington State, USA, was used to test the algorithm. These traveltimes were inverted for seismic velocities and interpreted for structure in a previous study (Brocher et al., 2001). We can thus readily assess the effects of incorporating the gravity algorithm.

Connected waterways in the Puget Lowland permitted an areal geophysical experiment in March 1998 called Seismic Hazards Investigation in Puget Sound (SHIPS), consisting of onshore-offshore wide-angle and multichannel seismic (MCS) reflection profiling throughout the Puget Lowland using an air gun array (Figure 3). The total volume of the air gun array varied between 110.3 litres and 79.3 litres, depending on whether wide-angle or MCS data were acquired. Wide-angle profiling was conducted throughout the study region, even in narrow waterways such as the Hood Canal and Lake Washington where the multichannel seismic streamer could not be towed (Fisher et al., 1999). MCS profiling was performed in Puget Sound and the Strait of Juan de Fuca (Figure 3). Air gun shot point locations and times accurate to a millisecond were determined from GPS navigation and GPS time recorded on the ship. The database includes 977,000 traveltimes picks from controlled sources.

The air gun shots were recorded by a temporary array of 210 seismographs deployed onshore and on the floor of Puget Sound (Figure 3) (Brocher et al., 1999). The SHIPS data were acquired with a shot spacing between 50 and 150 m and receiver spacing between 5 and 15 km. The quality of the wide-angle data obtained during SHIPS is highly variable, although most stations provided useful data to source-receiver offsets of at least 40-50 km. At bedrock sites remote from

urban centers, first arrivals can be observed to ranges up to 200 km. On the other hand, few interpretable data were recorded at some of the soft soil sites in urban or suburban localities.

The Puget Lowland of Washington is seismically active, and is crossed by many faults that offset Quaternary deposits, or that have a history of late Holocene rupture (Gower et al., 1985; Atwater and Moore, 1992; Bucknam et al., 1992; Johnson et al., 1994, 1996, 1999). Major crustal fault zones bound the Tacoma, Seattle, and Everett basins (Figure 3), large geological features that may prolong and amplify the strong ground motions. The Tacoma and Seattle basins introduce a significant difference in the delay times of first arrivals produced along shot lines in Puget Sound versus Hood Canal. In Puget Sound, traveltimes delays produced by the Seattle Basin exceed 1 s (Brocher et al., 2001).

### **Resolution and test models**

Resolution in seismic tomography depends on three properties of the problem: the signal band width, the source-receiver distribution, and the velocity structure itself. In this study we attempt to exploit the fact that in many areas, gravity data coverage is more uniform and more closely spaced than seismic source-receiver distribution, which should enhance resolution.

Three approaches are usually adopted to investigate resolution in tomographic problems. The simplest is a hit count analysis, where the number of rays sampling a given cell are examined to identify regions of good coverage and poor coverage. The second approach to resolution analysis is the construction of synthetic tests using the data distribution (Humphreys and Clayton, 1988). The synthetic test may be an attempt to construct point-spread functions, or to reconstruct the major features of the model simultaneously. The third common method of resolution analysis is the use of the resolution matrix of linear inverse theory. Typically the diagonals of the resolution matrix are displayed, and a certain value is chosen to indicate good resolution. The resolution matrix is a construct well suited to the study of linear problems, but extension to nonlinear problems is always questionable, particularly when the solution is approached iteratively (Shaw and Orcutt, 1986).

Each of the above resolution diagnostics depends on the velocity structure used to construct the resolution measures. Quantitatively connecting a hit count, synthetic test, or resolution matrix with the actual accuracy of the reconstructed image is not straightforward. A combination of these resolution indicators can provide some intuition into the resolving power of the data. We

have chosen to use a backprojection, and thus do not construct a formal resolution matrix. We instead show the hit count to illustrate the seismic ray coverage and use checkerboard tests to estimate the degree of uniqueness of the solution. The checkerboard tests were conducted by calculating synthetic traveltime picks between all the SHIPS source and receiver positions, and a synthetic gravity field with a model of 10x10 km columns, each with alternating increasing velocity gradients that were 0.5 km/s different at all depths. The synthetic traveltime picks and synthetic gravity grid were then used with a 1-D starting velocity model to recover the checkerboard pattern by sequential inversion, and compared with the result of using only the traveltime picks.

Results from resolution tests limited to seismic traveltimes show recovery of a smoothed version of the checkerboard pattern only in regions where seismic ray coverage is high (Figures 4, 5) (see also Brocher et al., 2001). Significant improvement is made by sequentially incorporating the gravity constraints, particularly in areas with minimal seismic coverage. The improvement is primarily recovery of the shape and scale of relative velocity variation rather than recovery of absolute velocities because a fixed velocity-density relation was used. Our estimated confidence in locating the actual boundaries improves with the addition of gravity; Brocher et al. (2001) estimated that anomalies greater than 15 km across were resolvable using only traveltimes. Here we conclude that 10-km anomalies are well resolved.

The checkerboard resolution tests indicate some utility of the gravity inversion in extending the model outside of the seismic coverage because the checkerboard pattern is recovered in those regions (Figure 4). Spatial smoothing of the model extends the influence of seismically determined velocities by the half-width of the smoother. Beyond this distance the gravity inversion is highly sensitive to the starting model velocity gradient and will tend to suggest sedimentary basins where the observed anomaly is low, and basement highs corresponding with gravity highs. Without some guidance from the starting velocity model, features such as low-density granitic plutons or high-density carbonates or mafic intrusions would probably be mishandled. Low-velocity zones are also unlikely to be properly resolved in areas lacking seismic coverage unless the starting model includes reverse gradients with depth.

## Application and evaluation

Resolution tests using synthetic data sets based on a real geometry show improvements to a velocity model by incorporating sequential gravity iterations. In this section we make a qualitative assessment using real traveltimes data from the SHIPS experiment and the observed gravity anomaly for the Puget lowland study area of Brocher et al. (2001) (Figures 3, 6). The gravity observations were discretized onto a surface grid of 1x1 km cells that corresponds to the 1-km cubes in the 3-D velocity model (Figure 6). The best results in terms of reducing traveltimes and gravity residuals were achieved by running 5 iterations using traveltimes only, and then introducing the gravity constraints sequentially with traveltimes iterations for another 5 iterations. Based on the distribution of seismic sources and receiver stations, we sought to resolve velocity anomalies ~5-10 km across in the lateral dimensions. We thus applied a 5-km halfwidth smoothing filter during the final iteration, which yielded an RMS traveltimes misfit of 0.09 s, and a 5 mGal RMS misfit to the gravity. Introduction of the gravity constraint necessitated some minor station corrections to achieve the 0.09-s RMS traveltimes misfit. At some stations, traveltimes misfits were consistently shifted either positively or negatively, without dependence on source azimuth and range; in these cases the mean traveltimes residual was subtracted from the RMS residual. Introduction of the gravity constraint caused this problem because seismic coverage is very sparse in the upper 1-2 km of the model, and lateral smoothing of nearby localized velocity anomalies affected velocity immediately beneath some stations.

### *Recovery of the gravity anomaly*

In Figure 6, a comparison of predicted gravity calculated from velocity models developed with and without sequential gravity steps is made. As expected, the velocity model calculated with gravity and seismic traveltimes reproduces more features of the observed gravity anomaly than does the traveltimes-only model. However, in one place the calculated anomaly does not match well with observed; the anomaly associated with the Tacoma Basin is reproduced only slightly better by the combined model. It appears that density is lower for a given velocity in the Tacoma Basin as compared with the Seattle Basin, where the calculated anomaly agrees well with observed (Figure 6). This circumstance indicates that in some cases, a spatially varying velocity-density relationship might be desired to best resolve structure.

### ***Comparison of velocity models with known geologic features***

The velocity model that resulted from sequential inversion of traveltimes and gravity is shown at 5-km depth in Figure 7, where a comparison is made between a model generated from the traveltime data only and one that was fit to traveltimes and the gravity anomaly. Evaluation of results from applying the sequential gravity steps to the SHIPS model is subjective because the actual subsurface structure is unknown. There are, however, some features in the combined model that appear better correlated with surface geology and inferred, related deeper structure. For example, the accreted sedimentary core of the anticlinal Olympic Mountains uplift is expected to have lower seismic velocity than their backstop, the Eocene volcanic rocks of the Crescent Formation that form a rim around the Olympic Mountains (e.g., Tabor and Cady, 1978; Parsons et al., 1999). The rim of high-velocity Crescent rocks is well resolved by the traveltime model, but there is only a limited image of lower-velocity Olympic core rocks inside the rim because of poor seismic coverage (Figures 5,7). With the incorporation of gravity, lower-velocity core rocks are more evident, and the rim of Crescent Formation rocks is resolved farther west than before.

Another example is the southern Whidbey Island fault, discussed by Johnson et al. (1996), which is resolved by the traveltime model as bounding the Seattle Basin on the southeastern end of the fault. The combined traveltime-gravity model shows additional influence of this fault on Whidbey Island, where a distinct high-velocity anomaly is bounded by the northwest extent of the southern Whidbey Island fault (Figure 7) that is not evident from the traveltime-only model. Much of this high-velocity anomaly occurs offshore where there are many airgun sources, but few receivers, causing unreversed seismic arrivals that limit resolution.

A final example is the Everett Basin, which is located north of the Seattle Basin and was poorly resolved by the traveltime model because it lies at the edge of seismic coverage (Brocher et al., 2001; Figures 5,6). Incorporation of the gravity observations introduces this basin into the velocity model where it was previously absent (Figure 7). Even relatively small gravity anomalies can have important effects on the velocity model in the upper crust where seismic coverage is sparse.

It appears that structures around the edges of seismic coverage are better resolved as a result of fitting the gravity anomaly (Figure 7). Subtle changes are also evident within the region of high coverage (Figures 5, 7) where the Tacoma Basin, and to a lesser extent, the Seattle Basin

have slightly different shapes. The resolution tests showed better recovery of the checkerboard pattern in the region of highest ray coverage (Figures 4, 5); the modifications to the Tacoma and Seattle basins may thus indicate refinement of these basins in the model though this is difficult to verify.

### ***Evaluation from borehole velocity data***

Six deep industry boreholes in our study area provide sonic velocity logs (Figure 3). Comparison of the tomography model to these sonic velocity logs suggests that the shallow (upper 3 km) velocities are generally well recovered by both velocity models (Figure 8). This comparison as originally made by Brocher et al. (2001) showed that the velocity structure in the upper 3 km of the traveltimes-only model matched the data from four of the six boreholes to within 0.2 to 0.3 km/s, particularly for the sedimentary rocks in the Oligocene Blakeley Formation filling the Seattle Basin. Thin (<300 m thick) layers of high-velocity Crescent Formation in the Socal Whidbey 1 and Pope and Talbot 18-1 boreholes were too thin to be resolved by the tomography method (Figure 8). The greatest misfit occurred at the Pope and Talbot 3-1 and Dungeness Spit 1 wells at the northern end of the tomography model in regions having sparse receivers (Figures 3, 8). Incorporation of gravity improved the fit to wells where seismic coverage was sparse, but degraded the fit slightly where seismic coverage was best, such as at the Mobil Kingston #1 well. This occurrence illustrates the trade-offs in seismic resolution that can result from the gravity constraint.

### ***Comparison of velocity models in cross-section view***

A cross-section (location shown in Figure 7) from the velocity model shows how structure was modified by the incorporation of gravity in the inversion. The differences are relatively minor, but potentially important (Figure 9). A deeper zone of low velocity beneath the Olympic Mountains was modeled, with a ~3-km downward shift of isovelocity contours resulting from the observed gravity low in the Olympic Mountains (Figure 6). A higher velocity at the surface is modeled where Crescent Formation volcanic rocks are exposed, and where seismic coverage is absent (Figure 9). The modeled shape of the Seattle Basin is changed with the incorporation of gravity; the basin appears more symmetric because the eastern edge is modified from the starting model and is better resolved where seismic coverage fades out. By design, most of the variation

occurs where seismic coverage is low or nonexistent. Resolution of basins near their edges may enable more accurate simulation of earthquake strong ground motion.

## Conclusion

We demonstrate improvement to synthetic and real 3-D seismic-velocity models by incorporating gravity modeling as a sequential step in travelttime inversion. The technique is simple and can be easily added to any iterative, grid-based travelttime modeling scheme. Inversions of seismic travelttimes and gravity observations have resolving power in different parts of the crust. Additionally, there are usually more gravity stations than seismic recorders in a given region, and the two data sets often have different spatial distribution. Thus, adding a gravity constraint as a sequential step in the seismic-velocity inversion can significantly improve resolution of shallow crustal structure.

**Acknowledgements** This study is cooperative between the USGS Earthquake Hazards, Geologic Mapping, and Coastal and Marine Programs. Gary Ernst, Michael Fisher, Simon Klemperer, and Vicki Langenheim and provided thoughtful review comments.

## References

- Achauer, U., 1992, A study of the Kenya rift using delay-time tomography analysis and gravity modeling, *Tectonophysics*, v. 209, p. 197-207.
- Atwater, B.F., and Moore, A. L., 1992, A tsunami about 1000 years ago in Puget Sound, Washington, *Science*, v. 258, p. 1614-1617.
- Blakely, R. J., 1995, *Potential theory in gravity and magnetic applications*, Cambridge, Cambridge University Press, 441 pp.
- Brocher, T.M., and Ruebel, A.L., 1998, Compilation of 29 sonic and density logs from 23 oil test wells in western Washington State, U.S. Geological Survey Open File Report, v. 98-249, 41 pp.
- Brocher, T.M., et al., 1999, Wide-angle seismic recordings from the 1998 Seismic Hazards Investigation of Puget Sound (SHIPS), western Washington and British Columbia, U.S. Geological Survey Open File Report, v. 99-314, 110 pp.
- Brocher, T.M., Parsons, T., Blakely, R. J., Christensen, N. I., Fisher, M. A., and Wells, R. E., 2001, Upper crustal structure in Puget Lowland, Washington: Results from the 1998 seismic hazards investigation in Puget Sound, *Journal of Geophysical Research*, v. 106, p. 13541-13564.
- Bucknam, R.C., Hemphill-Haley, E., and Leopold, E.B., 1992, Abrupt uplift within the past 1700 years at southern Puget Sound, Washington, *Science*, v. 258, p. 1611-1614.
- Fisher, M. A., Brocher, T. M., Hyndman, R. D., Trehu, A. M., Weaver, C. S., Creager, K. C., Crosson, R. S., Parsons, T., Cooper, A. K., Mosher, D., Spence, G., Zelt, B. C., Hammer, P. T., ten Brink, U., Pratt, T. L., Miller, K. C., Childs, J. R., Cochrane, G. R., Chopra, S., and Wailia, R., 1999, Seismic survey probes urban earthquake hazards in Pacific Northwest, *EOS*, v. 80, p. 13-17
- Gardner, G. H. F., Gardner, L. W., and Gregory, A. R., 1974, Formation velocity and density: the diagnostic basis for stratigraphic traps, *Geophysics*, v. 39, p. 770-780.

- Golizdra, G. Y., 1980, Statement of the problem of comprehensive interpretation of gravity fields and seismic observations, *Physics of the Solid Earth*, v. 16, p. 535-539.
- Gower, H.D., Yount, J.C., and Crosson, R.S., Seismotectonic map of the Puget Sound region, Washington, U.S. Geological Survey Miscellaneous Investigations Series Map, I-1613, scale 1:250,000, 1985.
- Hammer, P. T. C., 1991, Seamount structure from seismic tomography and gravity inversion, [Ph.D. Thesis] University of British Columbia, Vancouver, Canada, 174 pp.
- Hole, J. A., 1992, Nonlinear high-resolution three-dimensional seismic travel time tomography, *Journal of Geophysical Research*, v. 97, p. 6553-6562.
- Hole, J. A., and Zelt, B. C., 1995, 3-D finite-difference reflection traveltimes, *Geophysical Journal International*, v. 121, p. 427-434.
- Iyer, H. M., and Hirahara, K., 1993, *Seismic tomography theory and practice*, London, Chapman and Hall, 842 pp.
- Humphreys, E., and R. W. Clayton, 1988, Adaptation of back projection tomography to seismic travel time problems, *Journal of Geophysical Research*, v. 93, p. 1073-1085.
- Johnson, S. Y., Potter, C.J., and Armentrout, J.M., 1994, Origin and evolution of the Seattle fault and Seattle basin, *Washington, Geology*, v. 22, p. 71-74.
- Johnson, S. Y., Potter, C.J., Armentrout, J.M., Miller, J.J., Finn, C., and Weaver, C.S., 1996, The southern Whidbey Island fault, western Washington - An active structure in the Puget Lowland, *Washington, Geological Society of America Bulletin*, v. 108, p. 334-354.
- Johnson, S. Y., Dadisman, S.V., Childs, J.R., and Stanley, W.D., 1999, Active tectonics of the Seattle fault and central Puget Sound, Washington—Implications for earthquake hazards, *Geological Society of America Bulletin*, v. 111, p. 1042-1053.
- Langenheim, V. E., and Hauksson, E., 2001, Comparison between crustal density and velocity variations in southern California, *Geophysical Research Letters*, v. 28, p. 3087-3090.
- Lees, J. M., and VanDecar, J. C., 1991, Seismic tomography constrained by Bouguer gravity anomalies: applications in western Washington, *Pure and Applied Geophysics*, v. 135, p. 31-52.
- Lines, L. R., Schultz, A. K., and Treitel, S., 1988, Cooperative inversion of geophysical data, *Geophysics*, v. 53, p. 8-20.
- Luetgert, J. H., 1992, *MacRay-Interactive two-dimensional seismic raytracing for the Macintosh*, U. S. Geological Survey Open File Report, v. 92-356.
- Masson, F., Achauer, U., and Wittlinger, G., 1998, Joint analysis of P-traveltimes teleseismic tomography and gravity modeling for northern Tibet, *Journal of Geodynamics*, v. 26, p. 85-109.
- Oppenheimer, D. H., and Herkenhoff, K. E., 1981, Velocity-density properties of the lithosphere from three-dimensional modeling at The Geysers-Clear Lake region, California, *Journal of Geophysical Research*, v. 86, p. 6057-6065.
- Parsons, T., R. E. Wells, E. Flueh, U. S. ten Brink, and M. A. Fisher, 1999, Three-dimensional velocity structure of Siletzia and other accreted terranes in the Cascadia fore arc of Washington, *Journal of Geophysical Research*, v. 104, p. 18,015-18,039.
- Shaw, P. R., and Orcutt, J. A., 1986, Waveform inversion of seismic refraction data and applications to young Pacific crust, *Geophysical Journal of the Royal Astronomical Society*, v. 82, p. 375-414.
- Tabor, R. W., and Cady, W. M., 1978, The structure of the Olympic Mountains, Washington—analysis of a subduction zone, U. S. Geological Survey Professional Paper, v. 1033, 38pp.
- Vidale, J. E., 1990, Finite-difference calculation of traveltimes in three dimensions, *Geophysics*, v. 55, p. 521-526.

## Figure Captions

Figure 1. Comparison between observed velocity vs. density from Puget Lowland rock samples and the Gardner's rule (Garner et al., 1974) relation we use in sequential seismic traveltime and gravity inversion for crustal structure.

Figure 2. Comparison of velocity-depth profiles taken from 3-D models derived from seismic traveltimes only (black line) with combined analysis of traveltimes and gravity (gray line). Adjacent bar graph shows seismic hit count with depth associated with the velocity-depth curves.

Perturbation introduced by incorporating gravity is greatest where the velocity gradient is steepest (between 1-4 km depth) and where seismic coverage is sparse.

Figure 3. Location of Seismic Hazards Investigation in Puget Sound (SHIPS) seismographs (dots) and airgun tracks (dashed and solid lines) in Washington State, USA. Solid boxes show locations of deep wells with sonic velocity logs examined in this study.

Figure 4. Checkerboard resolution tests. Synthetic traveltimes and gravity observations were calculated with the input model using the SHIPS experiment geometry. The models recovered using traveltimes only and by combining traveltimes with observed gravity are shown at 5 km depth. Use of gravity in combination with seismic traveltimes resolves the checkerboard pattern much better than traveltimes alone, and over a larger area.

Figure 5. Comparison between distribution of gravity observations (small yellow dots) and seismic sources and receivers (dashed lines, blue dots) in the Puget Lowland. Gravity coverage is more uniform and the number of observation points is greater than the wide-angle recorders in the SHIPS seismic experiment. Also shown is seismic ray coverage at 5-km depth below sea level expressed as a hit count, the number of times a 1-km cubic cell in the model is crossed by seismic raypaths between sources and receivers. The darkest areas have the highest hit counts.

Figure 6. Calculation of the gravity anomaly from velocity models developed from (a) traveltimes only, and (b) combined traveltimes and gravity analysis. As expected, more features of (c) the observed gravity anomaly are apparent from the combined analysis. This exercise highlights areas like the Tacoma Basin, where the traveltimes residuals were satisfied, but the full gravity anomaly was not, implying that relatively lower density rocks for a given velocity may fill the basin.

Figure 7. Horizontal (map-view) slices from the 3-D model volumes at 5-km depth below sea level are shown from the traveltimes-only inversion (at left), and the combined gravity-traveltime inversion (at right). Incorporation of gravity highlights features not previously evident such as the Everett Basin, and offset of a high-velocity body along the northwest end of the South Whidbey Island fault. The image of low-velocity rocks of the Olympic Mountains ringed by higher-velocity, mafic Crescent Formation rocks is improved.

Figure 8. Comparison of tomography results with sonic log data and lithologies for six boreholes (Brocher and Ruebel, 1998; Brocher et al., 2001). Borehole locations are shown in Figure 3. The velocity profile from the model calculated from traveltimes only is shown with a heavy dashed line, and the velocity profile from combined traveltimes and gravity inversion is shown with a solid line.

Figure 9. Comparative east-west cross-sections from the 3-D velocity models derived from combined gravity and traveltimes analysis and from traveltimes modeling only (see Figure 6 for location). The region constrained by seismic raypaths is shown by the hit-count map below. The velocity structure is subtly changed by introduction of the gravity constraint: The low-velocity rocks of the Olympic Mountains are shifted deeper, and the eastern edge of the Seattle Basin is

more completely resolved. Slight variation in velocity structure beneath the depth of seismic coverage ( $\sim 15$  km) results mostly from smoothing conducted during the gravity inversion.

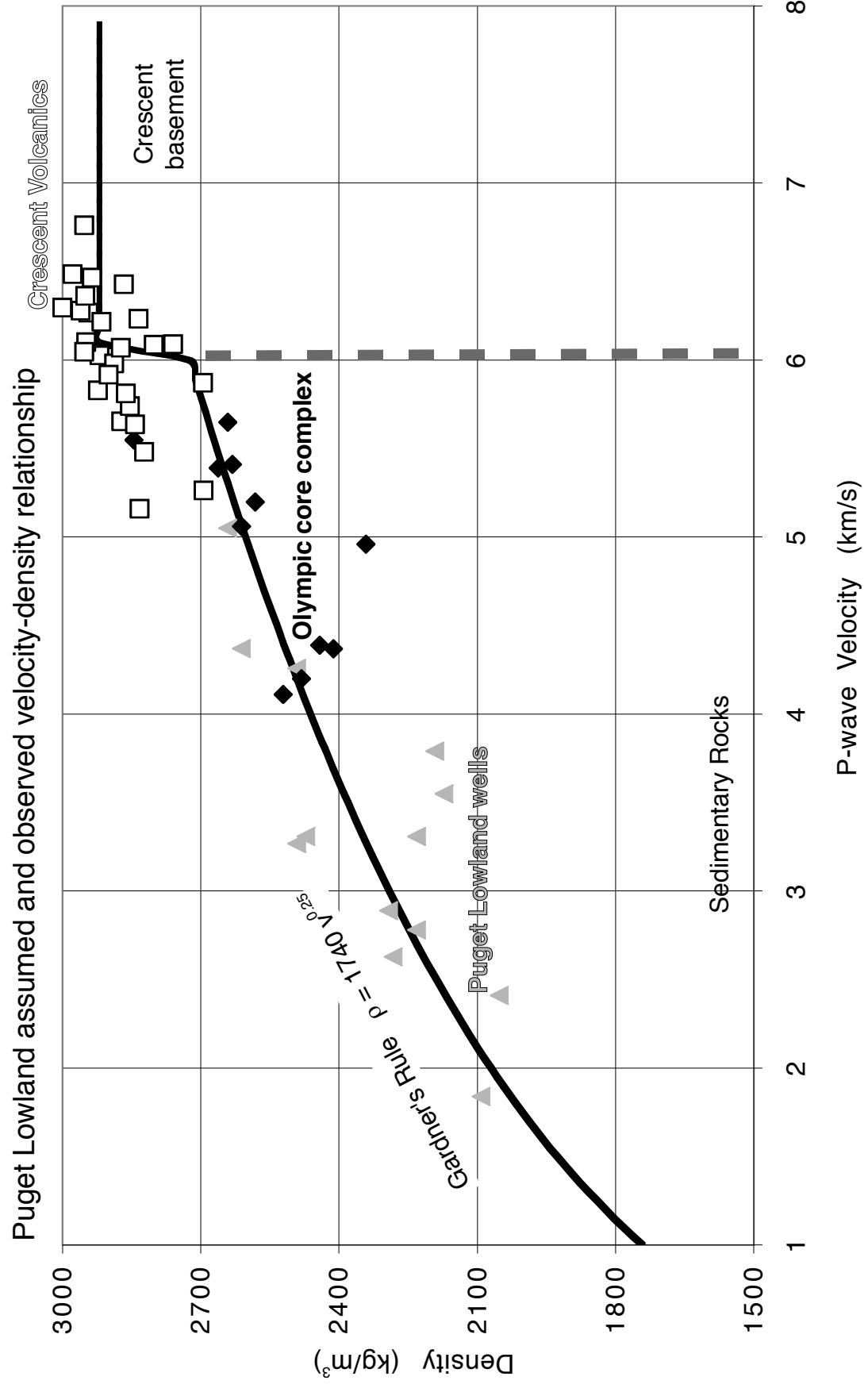


Figure 1

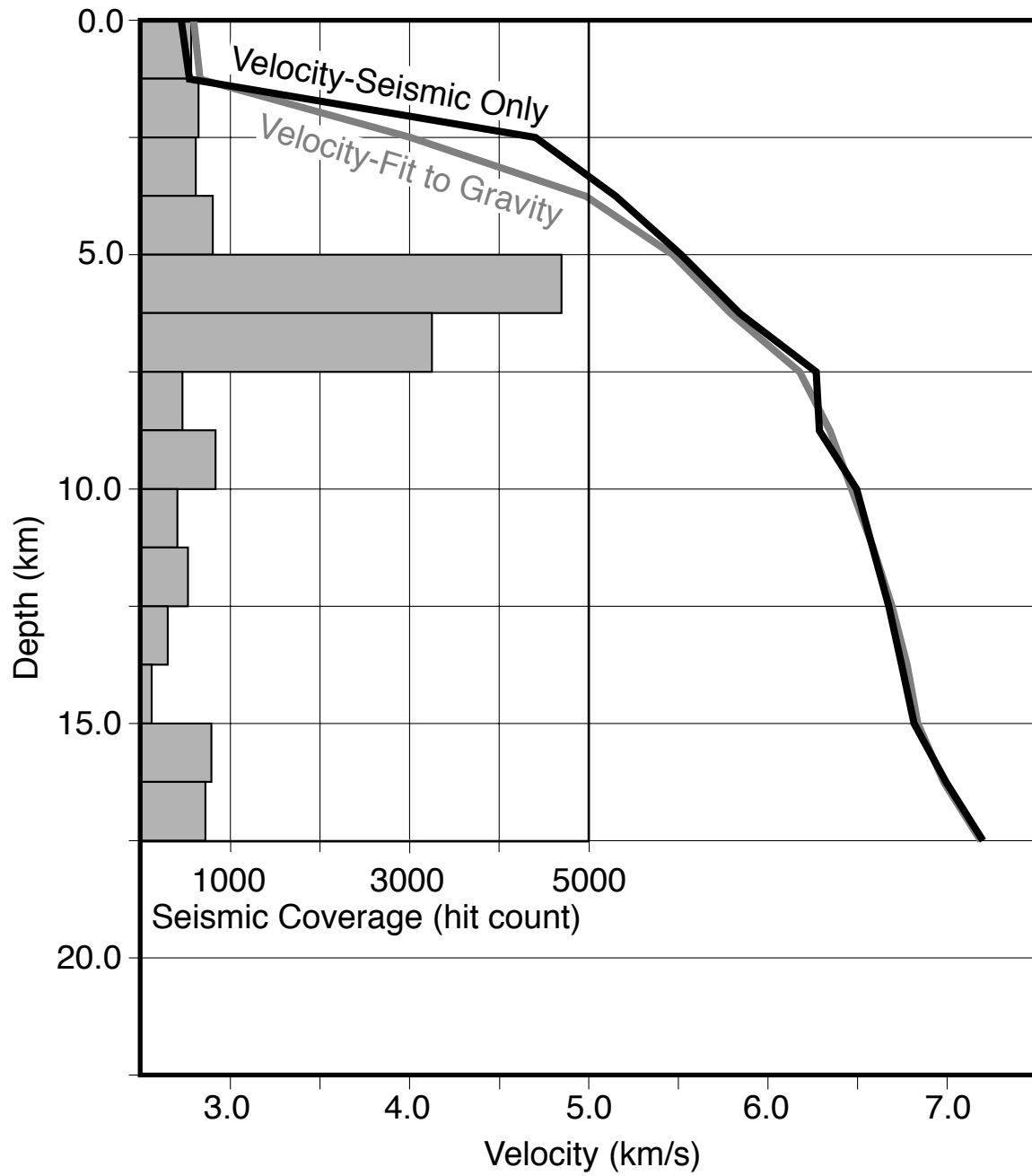


Figure 2

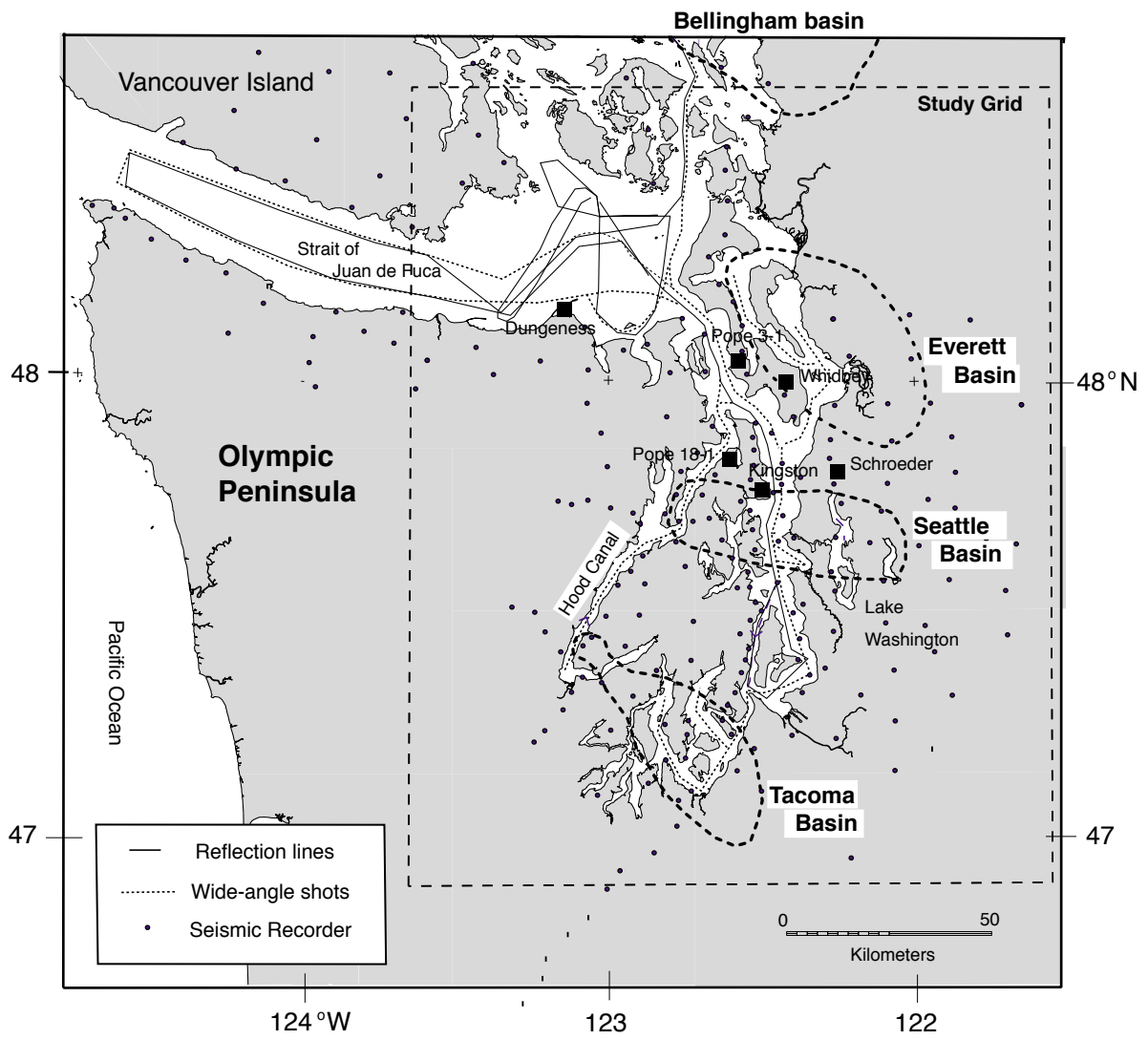


Figure 3



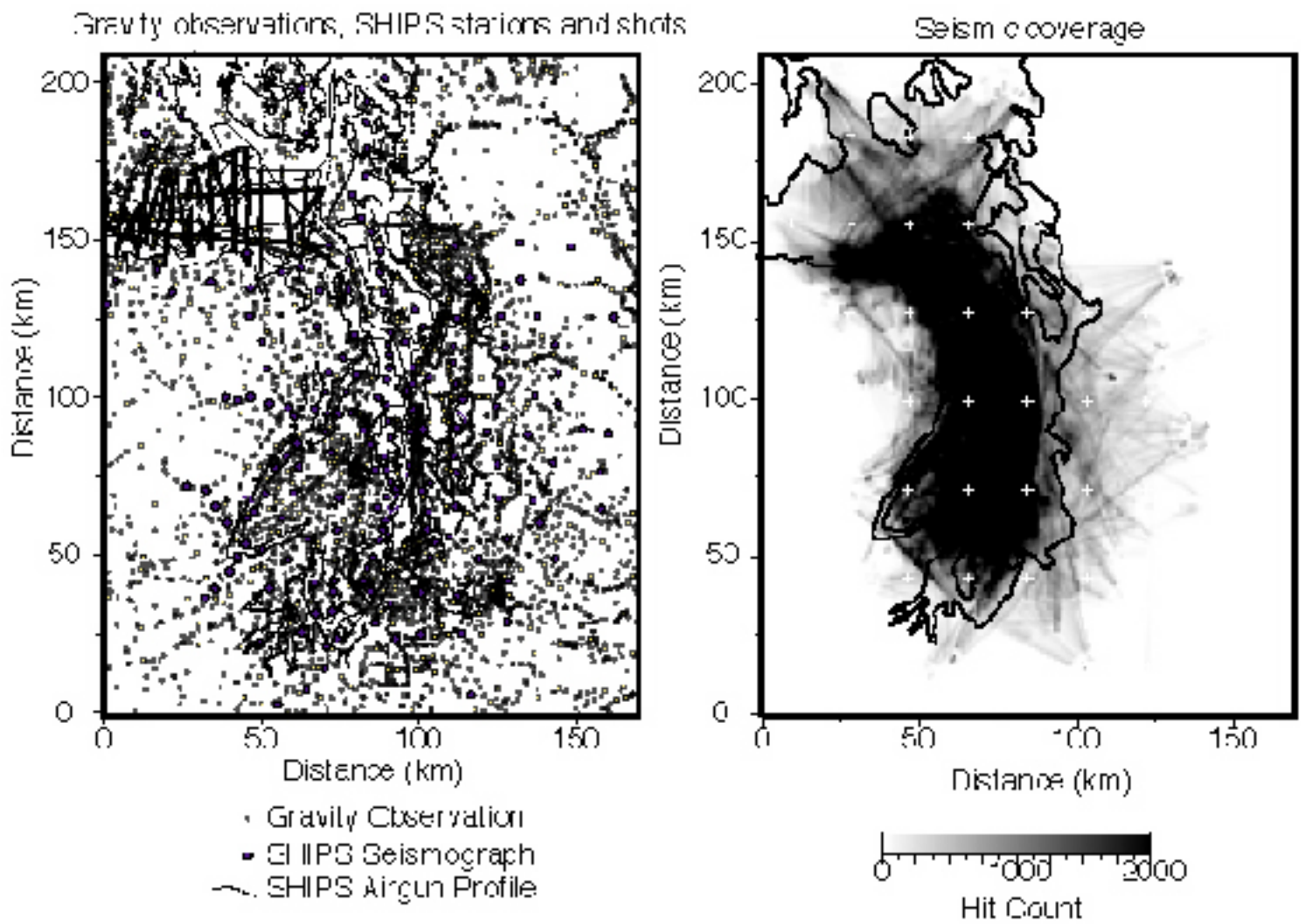


Figure 5

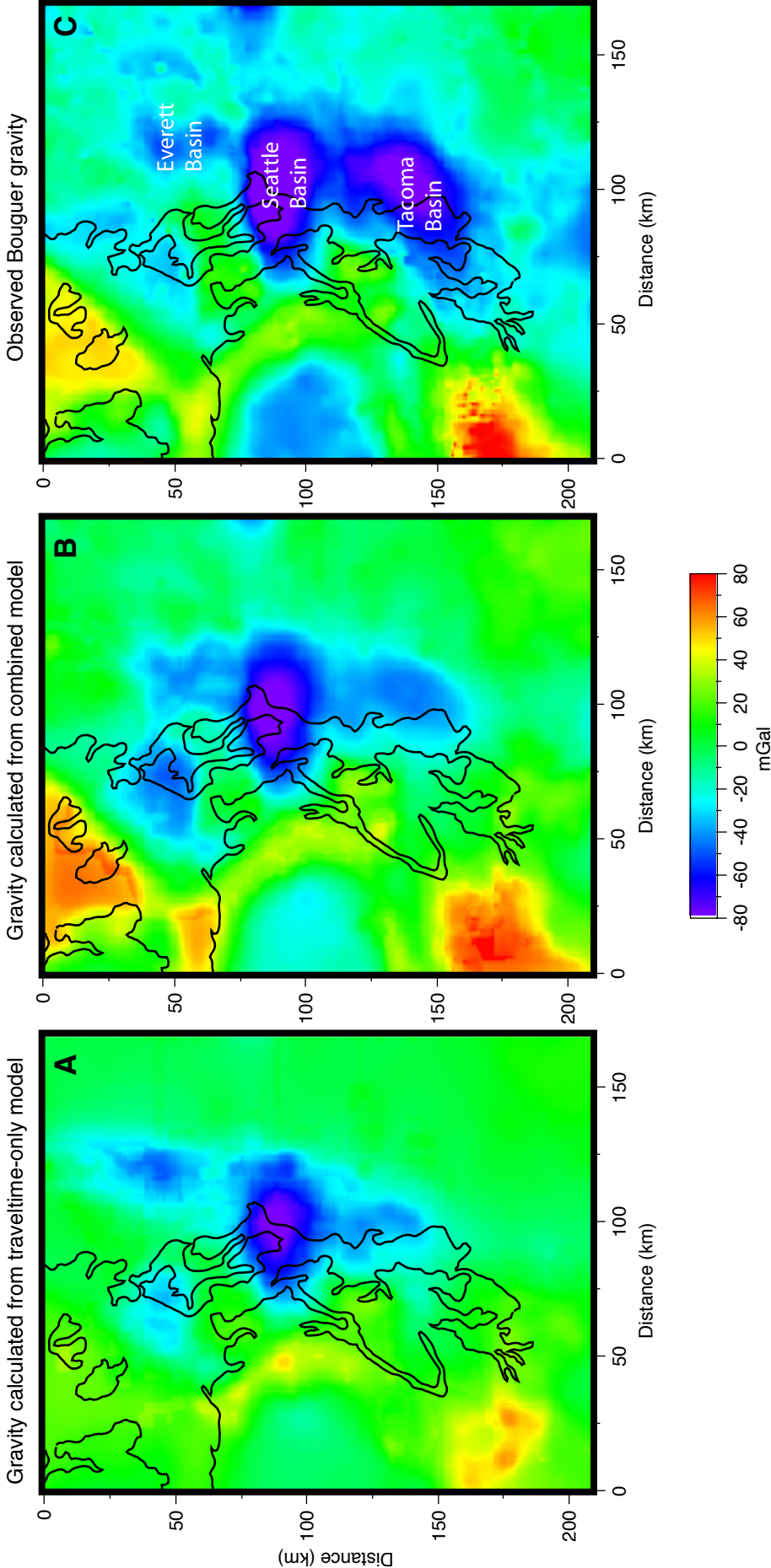


Figure 6

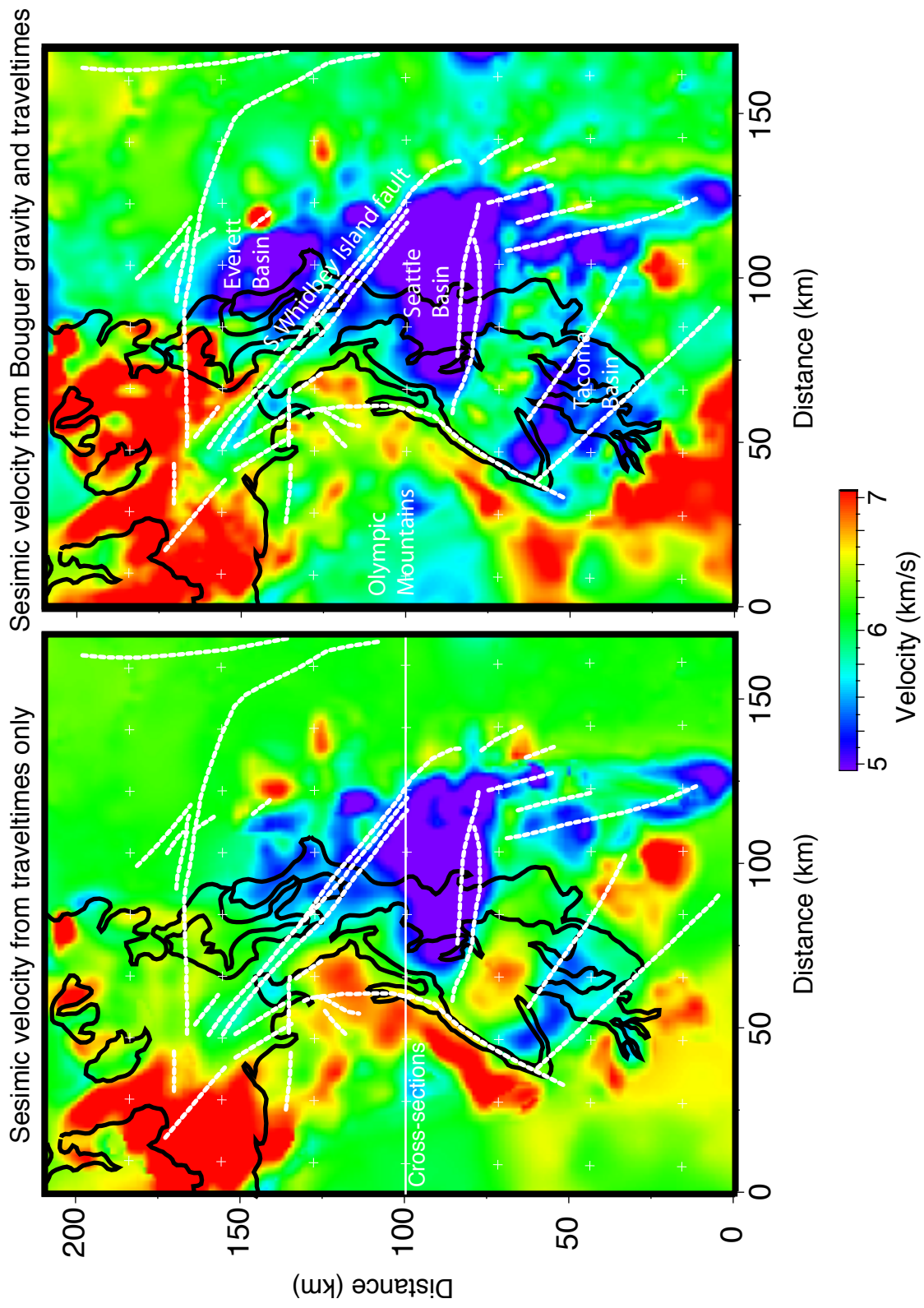
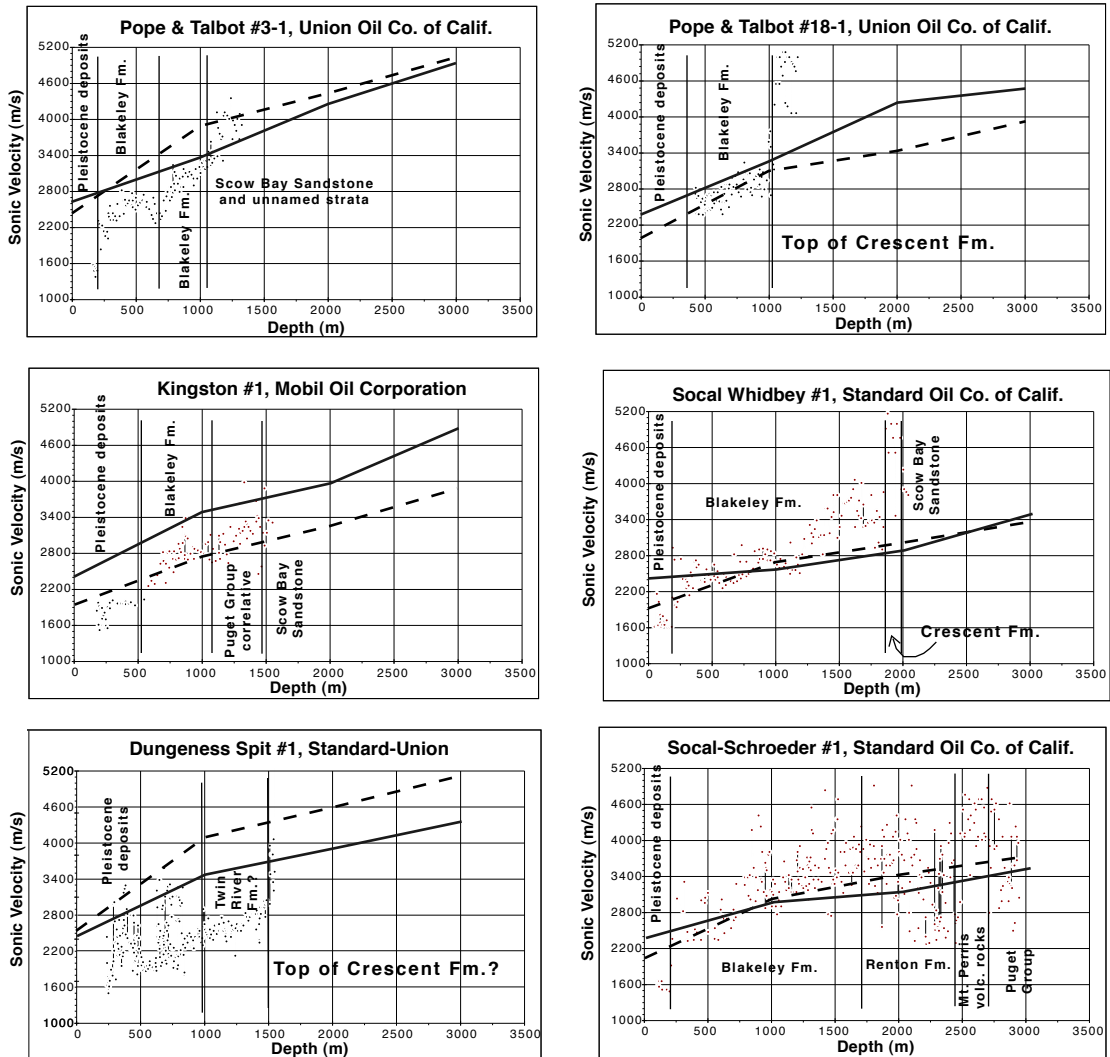


Figure 7



- - - - - Velocity-Depth Traveltime-only  
 \_\_\_\_\_ Velocity-Depth Gravity-Traveltime

Figure 8

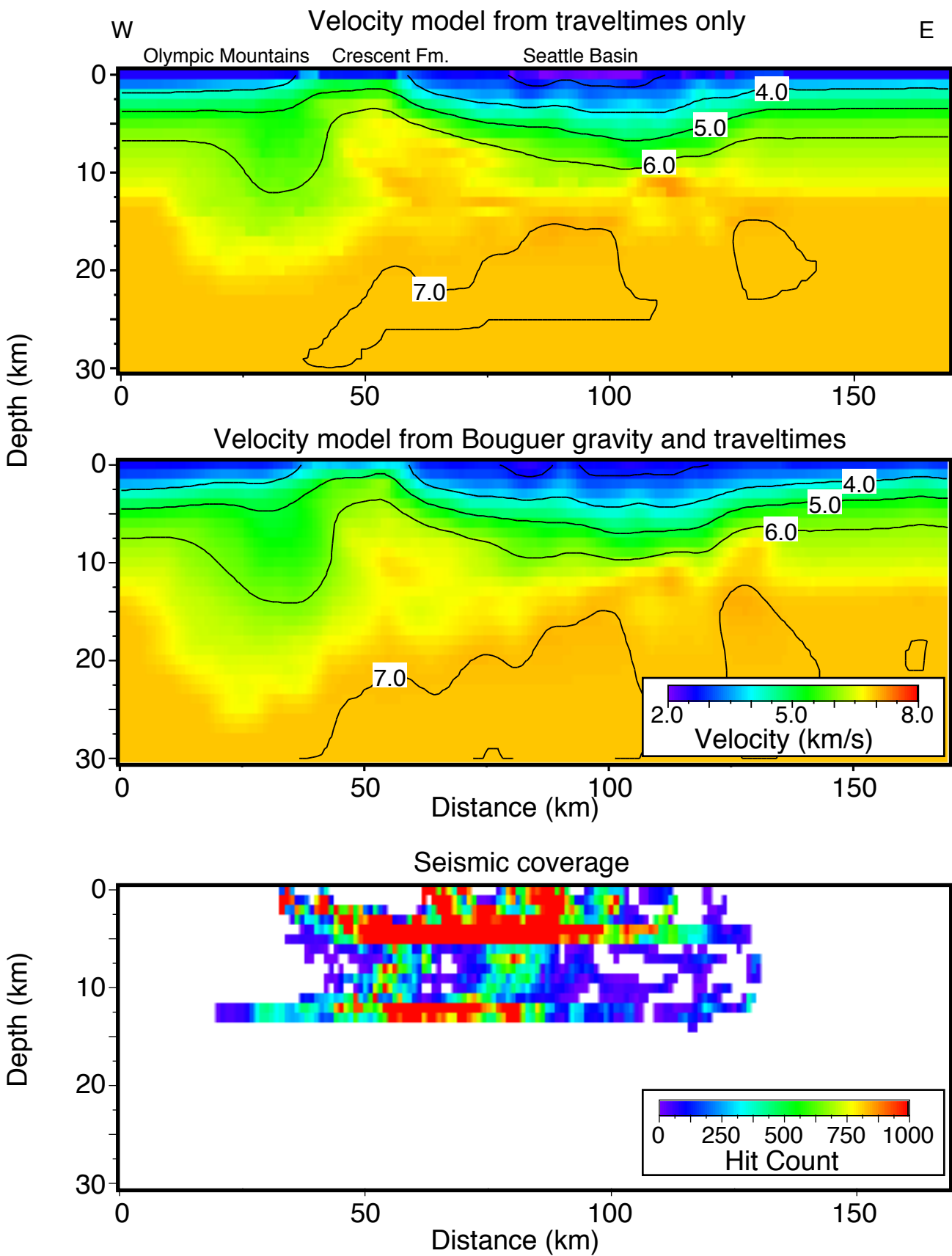


Figure 9